Modeling Friction and Air Effects between Cloth and Deformable Bodies

Zhili Chen*
The Ohio State University

Renguo Feng*
The Ohio State University

Huamin Wang*
The Ohio State University

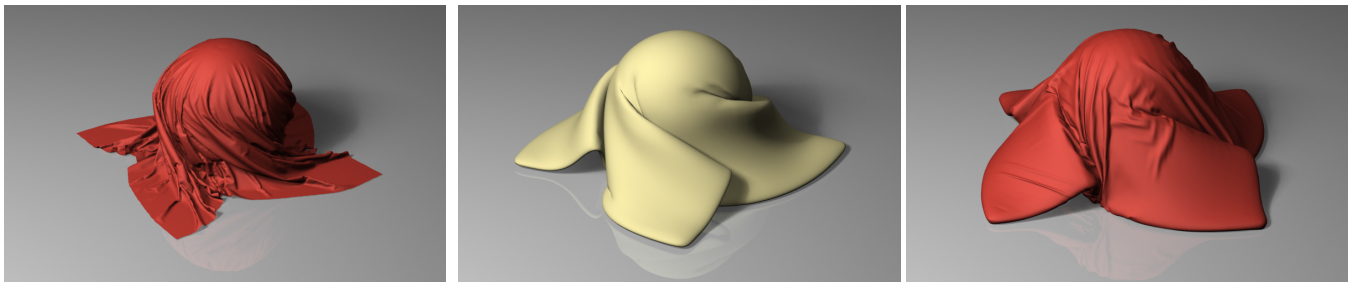

(a) Cloth only (b) Inner body only (c) Our model

Figure 1: *Rotating sphere. We propose efficient algorithms to realistically animate friction and air effects between cloth and deformable bodies. They allow us to simulate objects that are made of a cloth layer, an inner body layer, and an air layer. Compared with cloth animation in (a) and inner body animation in (b), the animation of such objects exhibit different dynamic behaviors as shown in (c).*

Abstract

Real-world cloth exhibits complex behaviors when it contacts deformable bodies. In this paper, we study how to improve the simulation of cloth-body interactions from three perspectives: collision, friction, and air pressure. We propose an efficient and robust algorithm to detect the collisions between cloth and deformable bodies, using the surface traversal technique. We develop a friction measurement device and we use it to capture frictional data from real-world experiments. The derived friction model can realistically handle complex friction properties of cloth, including anisotropy and nonlinearity. To produce pressure effects caused by the air between cloth and deformable bodies, we define an air mass field on the cloth layer and we use real-world air permeability data to animate it over time. Our results demonstrate the efficiency and accuracy of our system in simulating objects with a three-layer structure (i.e., a cloth layer, an air layer, and an inner body layer), such as pillows, comforters, down jackets, and stuffed toys.

Keywords: Contacts, data-driven, material measurement, collision detection, air permeability, cloth simulation.

CR Categories: I.3.7 [Computer Graphics]: Three-Dimensional Graphics—Animation.

Links: DL PDF

*e-mail: {chenzhi, fengr, whmin}@cse.ohio-state.edu

1 Introduction

In the real world, cloth is often used as a cover to protect its interior from separation, moisture, heat, and dust. For bedding and clothing, the interior is made of soft materials that feel comfortable and warm. Animating the cloth cover and its interior requires a simulator to solve not only cloth and deformable body dynamics, but also their interactions. While graphics researchers have made substantial progress in simulating and modeling cloth [Wang et al. 2011; Zheng and James 2012; Miguel et al. 2012] and deformable bodies [Bickel et al. 2009; Faure et al. 2011; Coros et al. 2012] recently, how to efficiently and accurately handle their interactions is still a less studied problem. Many cloth animation effects, such as wrinkles and folds, are formed when cloth contacts itself or other objects. Without accurately handling the contacts, we cannot faithfully produce interesting cloth behaviors as in Figure 1.

The challenges in simulating the contacts between cloth and deformable bodies come from two main reasons. Firstly, a cloth cover frequently collides with its inner deformable body, making the collision detection process more computationally expensive. Such collisions often occur coherently in space and time, while self collisions of cloth are less common. We think these properties can be used to improve the efficiency of collision detection in this cloth-body interaction problem. Secondly, the contact behaviors of cloth and deformable bodies are highly complex in the real world, due to different combinations of cloth and deformable body materials. For example, their frictions can be nonlinear, anisotropic, and even asymmetric. The air trapped between cloth and deformable bodies provides more interesting effects in cloth animation, but it also requires more computational cost to simulate using fluid dynamics. How to model these behaviors and how to incorporate them into existing simulators have not been well studied in computer graphics or textile engineering yet, as far as we know.

We present a systematic study on efficiently and accurately animating contact behaviors between cloth and deformable bodies. The goal of our study is to simulate real-world objects that can be modeled by a three-layer structure, including a cloth cover as its outer layer, a deformable body as its inner layer, and an in-between air layer. Under this representation, we develop novel techniques to model and simulate cloth-body interaction from three aspects: collision, friction, and air pressure. Our main contributions are:

- A surface-traversal-based collision detection algorithm that runs significantly faster than alternative methods. It is more effective in frequent contact cases, and its results are useful in handling friction and air effects.
- A nonlinear, anisotropic friction model. We capture frictional data using a friction measurement device. Our dataset includes multiple cloth and deformable body materials, such as cotton, leather, and sponge.
- An air mass field representing the air layer. We update this field by an air propagation model and an air transfer model, the latter of which animates air penetrating through cloth using real-world air permeability data from [Cay et al. 2007].

The proposed models and techniques are compatible with most existing cloth and deformable body simulators. We implement a system based on them and we test its performance in cloth animation examples. Our experiment shows that this system can efficiently and realistically handle a variety of real-world objects with a three-layer structure, such as pillows (in Figure 3), comforters (in Figure 12b), and down vests (in Figure 12c).

2 Previous Work

Collision and Contact Handling. Collision handling is a large research area in computer graphics and previous research has studied a number of problems, including collision culling [Schvartzman et al. 2010; Lauterbach et al. 2010; Tang et al. 2011; Zheng and James 2012], collision detection [Provot 1997; Bridson et al. 2002; Stam 2009; Brochu et al. 2012], and asynchrony [Thomaszewski et al. 2008; Harmon et al. 2009; Ainsley et al. 2012]. While most previous techniques were developed for general collision cases, our collision detection algorithm was specifically designed to handle collisions between two surfaces that are in frequent contacts. Like other discrete approaches [Baraff et al. 2003; Wicke et al. 2006], it detects and resolves collisions at the end of each time step. It is efficient and robust, when objects are not moving too fast.

A more general question is how to animate complex contacts between two objects. Frictions are typically modeled using Coulomb's law, as Bridson and colleagues [2002] showed. Pabst and collaborators [2009] proposed a friction tensor to model anisotropic friction effects. Adhesive contacts can be modeled either by adhesive constraints [Bridson et al. 2002; Gascón et al. 2010], or adhesive springs [Jimenez and Luciani 1993]. Adhesive springs can also be used to handle the contacts between wet cloth and other objects as Huber and collaborators [2011] demonstrated. Shinar and colleagues [2008] developed a unified time integrator to simulate the contacts between deformable and solid bodies. Guendelman and collaborators [2005] studied the contacts between cloth and liquids. Lenaerts and colleagues [2008] used smoothed-particle hydrodynamics to animate fluids penetrating through porous deformable objects. By assuming that incompressible fluid exists virtually between two objects, Sifakis and collaborators [2008] solved fluid dynamics to calculate contact responses. Stam [2009] modelled inflation and deflation effects using uniform air pressure. In contrast, the air pressure force in our system is derived from a time-varying air mass field, which is updated due to air transfer and propagation. Using it, we can conveniently handle open cloth meshes and animate wavy effects on cloth.

Material Measurement. Material measurement has been an active research topic in computer graphics in recent years. The seminal work of Pai and colleagues [2001] pioneered this area by capturing and modeling a 3D deformable object's shape, elasticity, and friction properties. Their idea was later extended by Lang and collaborators [2002] for more robustness, and by Schoner and colleagues [2004] for visco-elasticity. While cloth material properties can also be obtained from unconstrained cloth motions as shown in [Bhat et al. 2003; Kunitomo et al. 2010], it turns out to be a much more difficult problem due to self occlusion and large deformation. Instead, Wang and collaborators [2011] and Miguel and colleagues [2012] developed their own 2D testers to measure nonlinear, anisotropic elasticity behaviors of cloth. The nonlinearity also exhibits in the elasticity of 3D objects, and Kauer and collaborators [2002] proposed a way to measure it. Bickel and collaborators [2009] pushed this direction even further by considering both nonlinearity and heterogeneity of 3D objects.

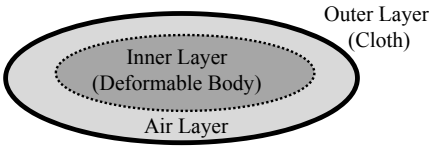

Figure 2: *A three-layer structure. It includes an outer cloth layer, an inner deformable body layer, and an air layer. The cloth layer may or may not be closed.*

Researchers in materials science and textile engineering have also developed a number of material measurement devices, such as tensile testers [KATO Tech 2013b; Deben 2013], bending testers [KATO Tech 2013a; Taber Industries 2013], and air permeability testers [Textest 2013; Frazier 2013; SDL Atlas 2013]. By using a vacuum pump to create desired pressure difference and a flowmeter to measure the amount of air passing through the test sample, most air permeability testers are designed in a Shirley test fashion and some of their results [Cay et al. 2007] are publicly available online. While researchers have also designed friction testers [KATO Tech 2013c; Qualitest 2013], existing friction datasets are still too limited for graphics research, due to various combinations of different materials. For this project, we are interested in not only self friction properties of cloth materials, but also the friction properties between cloth and deformable body materials, such as cotton, sponge, and leather.

3 A Three-Layer Structure

Our system is based on a three-layer structure, as Figure 2 shows. The outermost layer is a cloth cover. It is represented by a triangle mesh and it may not be closed. We use an implicit FEM solver to simulate its planar deformation, similar to Volino and collaborators [2009] did. We calculate the bending forces using the hinge edge model proposed by Bridson and colleagues [2002]. Both planar and bending stiffness parameters are chosen from the cloth elasticity database presented by Wang and collaborators [2011]. The innermost layer is an airtight deformable body. Since its shape is usually smooth, we represent it by a low-resolution tetrahedral mesh and simulate it by co-rotational FEM [Müller et al. 2002]. Between the cloth cover and the deformable body, we have an air layer represented by an air mass field. In each simulation time step, we first simulate the cloth layer and the inner layer separately, and then process their collisions (in Section 4) and frictions (in Section 5). After that, we update the air layer and apply its influence on the cloth layer and the inner body layer (in Section 6). Figure 3 shows the effects of this three-layer structure in a pillow example.

4 Collision Handling

We use the signed distances between cloth and deformable bodies to resolve their collisions in our system. In addition, the distances

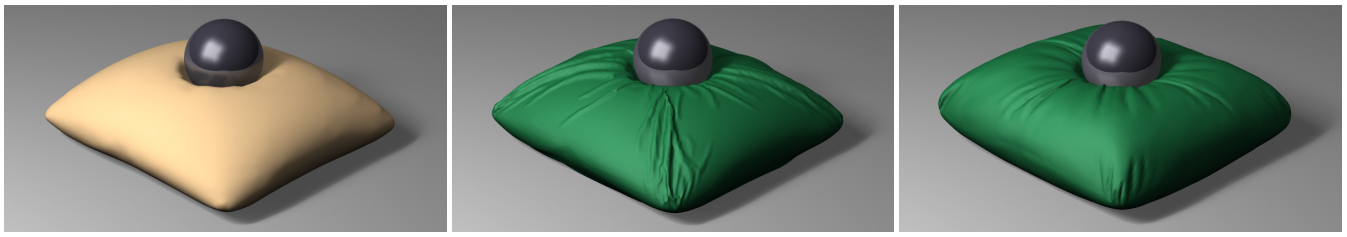

(a) Inner body only (b) Without the air layer (c) With the air layer

Figure 3: *A pillow. In this example, we compare the animation effects of using different layers. The inner body tends to have a smooth surface as (a) shows, while the cloth layer can provide interesting details as shown in (b). Using the air layer, different dynamic details are generated as (c) shows. The trapped air will gradually escape the pillow, and the cloth surface will become similar to (b) eventually.*

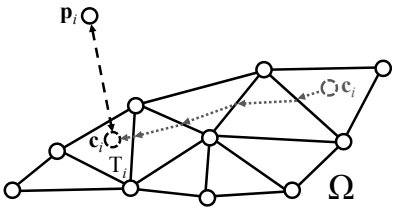

Figure 4: *Surface traversal. The point* $\mathbf{c}_i$ *travels from its initial location to its final location, which may be* $\mathbf{p}_i$*'s closest point on* $\partial\Omega$*.*

are used later in Section 5 and 6 to produce friction and air effects. Since collision detection is often the computational bottleneck, we propose a fast discrete collision detection algorithm in this section.

4.1 Discrete Collision Detection

Because the cloth mesh is typically in higher resolution than the deformable body mesh, our collision detection algorithm is focused on finding the collision between each cloth vertex and the deformable body. We will discuss how to avoid other collisions in Subsection 4.2. Given a cloth vertex $\mathbf{p}_i$ and the deformable body Ω, the goal is to locate $\mathbf{p}_i$'s closest point $\mathbf{c}_i$ on the deformable body boundary $\partial\Omega$, so that we can use $\mathbf{c}_i$ to calculate the signed distance from $\mathbf{p}_i$ to $\partial\Omega$. The distance is positive, when $\mathbf{p}_i \notin \Omega$; and negative, when $\mathbf{p}_i \in \Omega$. The surface traversal method finds $\mathbf{c}_i$ in a gradient descent fashion, as Figure 4 shows. Let $\mathbf{c}_i$ be assigned with an initial location on $\partial\Omega$ first and $\mathbf{c}_i$ is in triangle T_i. We calculate the projection of $\mathbf{p}_i$ on T_i's plane as $\mathbf{p}_i'$, and then move $\mathbf{c}_i$ toward $\mathbf{p}_i'$. If $\mathbf{c}_i$ hits an edge of T_i, we set T_i as the other triangle adjacent to that edge, update $\mathbf{p}_i'$, and continue this process. Surface traversal stops when $\mathbf{c}_i = \mathbf{p}_i'$, or the next triangle has already been visited. Intuitively, this method constantly drags $\mathbf{c}_i$ toward $\mathbf{p}_i$, while constraining $\mathbf{c}_i$ in $\partial\Omega$. When $\mathbf{c}_i$ stops moving, it becomes a local minimum of the distance function from $\mathbf{p}_i$ to $\partial\Omega$. If $\mathbf{c}_i$ is also the global minimum, we can then use the normals to determine the sign of the distance and whether $\mathbf{p}_i$ is inside of Ω.

Unfortunately, surface traversal cannot guarantee $\mathbf{c}_i$ to be the global minimum. To avoid collisions from being missed because of this, we formulate our collision detection algorithm as Algorithm 1 shows. Suppose that no penetration exists at time t and the time step is 1. Let U be the maximum relative speed. If a cloth vertex $\mathbf{p}_i$ collides with $\partial\Omega$ at a certain point between time t and $t+1$, then the distance between $\mathbf{p}_i^{t+1}$ and that point must be bounded by U. Therefore, the distance between $\mathbf{p}_i^{t+1}$ and $\partial\Omega^{t+1}$ must also be bounded by U. Let $\mathbf{S} \subset \partial\Omega^{t+1}$ be the set of triangles whose bounding box distances to $\mathbf{p}_i^{t+1}$ are less than or equal to U. If $\mathbf{p}_i^{t+1} \in \Omega^{t+1}$, then the

Input : A cloth vertex $\mathbf{p}_i^{t+1}$ and the deformable body Ω^{t+1}
Output: The signed distance d_i^{t+1}

Calculate $\mathbf{c}_i^{t+1}$ using surface traversal;
Calculate d_i^{t+1}, the signed distance from $\mathbf{c}_i^{t+1}$ to $\mathbf{p}_i^{t+1}$;
Update $\mathbf{c}_i^{t+1}$ and d_i^{t+1} by `Distance_Update`($\mathbf{p}_i^{t+1}$, $\mathbf{c}_i^{t+1}$, d_i^{t+1});

Algorithm 1: `Intersection_Test`($\mathbf{p}_i^{t+1}$)

Input : A cloth vertex $\mathbf{p}_i^{t+1}$, and its $\mathbf{c}_i^{t+1}$ and d_i^{t+1}
Output: The updated $\mathbf{c}_i^{t+1}$ and d_i^{t+1}

```
for every triangle T in ∂Ω^{t+1} do
    if visited[T] = 0 and Distance(Bound(T), p_i^{t+1})) ≤ U then
        if d_i^{t+1}'s sign is inconsistent with T then
            visited[T] ← 1;
            Calculate c, the closest point on T to p_i^{t+1};
            Calculate d, the signed distance from c to p_i^{t+1};
            if |d| < |d_i^{t+1}| then
                Update c_i^{t+1} and d_i^{t+1} by c and d;
                if d_i^{t+1} changed its sign then
                    Distance_Update(p_i^{t+1}, c_i^{t+1}, d_i^{t+1});
                    return;
                end
            end
        end
    end
end
```

Algorithm 2: `Distance_Update`($\mathbf{p}_i^{t+1}$, $\mathbf{c}_i^{t+1}$, d_i^{t+1})

closest point to $\mathbf{p}_i^{t+1}$ must be in $\mathbf{S}$. So when $\mathbf{S} = \emptyset$, no collision occurs. When $\mathbf{S} \neq \emptyset$, we first trace $\mathbf{c}_i^{t+1}$ from $\mathbf{c}_i^t$ using surface traversal and calculate the signed distance d_i^{t+1} from $\mathbf{c}_i^{t+1}$ to $\mathbf{p}_i^{t+1}$. Then for every triangle T in $\mathbf{S}$ that has not been visited yet, we test whether $d_i^{t+1} < 0$ but $\mathbf{p}_i^{t+1}$ is on the exterior side of T, or $d_i^{t+1} > 0$ but $\mathbf{p}_i^{t+1}$ is on the interior side of T. If such a inconsistency happens, we visit T by calculating the closest point $\mathbf{c}$ on T to $\mathbf{p}_i^{t+1}$. If $\mathbf{c}$ is closer than $\mathbf{c}_i^{t+1}$, we replace $\mathbf{c}_i^{t+1}$ by $\mathbf{c}$ and update d_i^{t+1} accordingly. If d_i^{t+1} changes its sign, we restart our search over $\mathbf{S}$. The algorithm ends if each triangle in $\mathbf{S}$ is either visited, or consistent with d_i^{t+1}'s sign.

The idea behind this algorithm is: we can tolerate if $\mathbf{c}_i^{t+1}$ is not the closest point, but we cannot tolerate if the sign of d_i^{t+1} is wrong. Let $\mathbf{c}$ be the closest point to $\mathbf{p}_i^{t+1}$. There must exist a triangle T (for $\mathbf{c} \in T \in \mathbf{S}$), such that $\mathbf{p}_i^{t+1}$ is on the exterior side of T when $\mathbf{p}_i^{t+1} \notin \Omega^{t+1}$, or $\mathbf{p}_i^{t+1}$ is on the interior side of T when $\mathbf{p}_i^{t+1} \in \Omega^{t+1}$. So if all triangles are consistent with $\mathbf{d}_i^{t+1}$'s sign, we know the sign must be correct. Using this idea, our algorithm guarantees that a collision

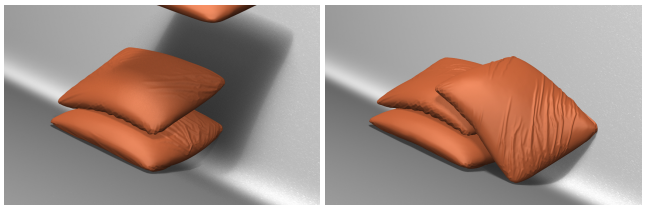

Figure 5: *Three Pillows. Intensive collisions happen between cloth and deformable bodies in this example. We use this example to test the performance of our collision detection algorithm.*

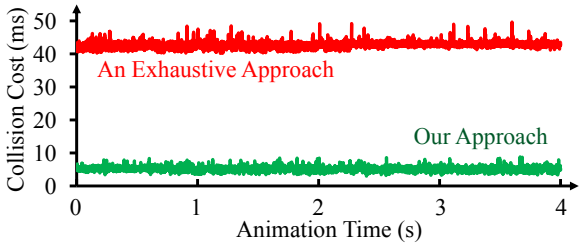

Figure 6: *Collision detection timings per time step. Our method runs approximately eight times faster than an exhaustive method.*

must be detected if $\mathbf{p}_i^{t+1}$ is inside of Ω^{t+1}. As a discrete method, it may still miss collisions when vertices quickly travel through the body, known as the tunneling artifact. The only solution to this problem under the discrete framework is to use smaller time steps, as far as we know.

Analysis. The efficiency of our algorithm comes from two reasons. Firstly, surface traversal explores collision coherence in space and time. When a cloth vertex slides over a deformable body, only a small set of triangles need to be examined. In extreme, when there is no relative motion between cloth and a deformable body, only one triangle needs to be tested per cloth vertex. Secondly, the deformable body mesh is smooth in most cases. A cloth vertex is likely to be on the exterior sides of most local triangles, if it is outside; and it is likely to be on the interior sides of most local triangles, if it is inside. If so, the only additional computational cost to surface traversal is a dot product per cloth vertex per local triangle.

Figure 6 compares the performance of our approach with the performance of an exhaustive approach, which calculates the vertex-triangle distance using every triangle in $\mathbf{S}$. Both approaches use a uniform grid acceleration structure and the comparison is based on a three pillow example containing 70K triangles as Figure 5 shows. In average, the surface traversal step in our approach visits only 1.4 triangles in each time step and the whole approach runs approximately eight times faster. Without using our method, our experiment shows that collision handling can cause more than 80 percent of the computational cost, at least half of which is spent on handling cloth-body collisions. So the use of our method can save approximately 30 to 40 percent of the overall computational cost.

Another advantage of our method is its ability to estimate the signed distance even when a vertex is far from the inner body. Although this distance may not be accurate, it is required in the air mass field update (in Section 6). For this reason, alternative approaches, such as the edge-triangle test [Baraff et al. 2003] and the ray-intersection test, do not fit in our system.

4.2 Other Steps

The collision detection algorithm described in Subsection 4.1 considers the collisions between cloth vertices and deformable bodies only. But there can be other cloth-body collisions, including the collisions between body vertices and cloth, and the collisions between cloth edges and body edges. To prevent them from causing penetration artifacts, we add a thickness buffer $H = 2L/3$ on the deformable body surface, in which L is the upper bound on cloth edge lengths. We typically set L from 2 to 5mm and we enforce it using the strain limiting method. By ensuring that the distances between cloth vertices and the deformable body are above $2L/3$, the algorithm guarantees that no other collisions can occur between cloth and deformable bodies.

We resolve the collision between a cloth vertex and a deformable body in the same way as Bridson and colleagues [2002] did. Specifically, given a distance coefficient h, if $d_i^{t+1} < H + h$, we apply repulsion forces on the vertex and the deformable body triangle. If $d_i^{t+1} < H$, we apply geometric constraints to prevent them from actual collision. When there are multiple collisions, we apply the constraints in a Jacobi fashion iteratively. Since most deformable body surfaces are smooth, this method often converges in one or two iterations and we did not experience any convergence issue. But if necessary, the impact zone method can be implemented in the future to avoid further collisions after a number of iterations.

5 Friction Effects

Real-world cloth has complex friction behaviors, including nonlinearity and anisotropy. Here we perform an experimental study to reveal these properties and we propose a simple friction model to animate friction effects in animation.

5.1 Friction Test

Our frictional test device is set up as Figure 7 shows. We place the cloth sample on the test bed and we attach the deformable body sample on the bottom of a weight cart. The friction between them happens when a linear actuator drives a sliding piece to move. The friction force is measured by a Futek LSM250 load cell sensor, attached between the sliding piece and the weight cart. We can modify the pressure forces between cloth and deformable bodies by using different weights on the cart. At the beginning of each test, the sample typically experiences a large friction force due to static friction. After that, the motion stabilizes and the dynamic friction force is nearly constant.

Figure 9a compares the friction forces of different cloth materials, when they contact sponge under a 0.05kg load. Figure 9b compares the friction forces of different deformable bodies, when they slide over the same Jet Set cloth material under a 0.1kg load. These two examples demonstrate the importance of frictional tests. Without real-world frictional data, we can only estimate friction coefficients in simulation, which are often far from accurate. Figure 9c and 9d illustrate the friction behaviors of the same cloth sample, when it is placed on the test bed with different orientations. Figure 9c shows that the friction between sheepskin and the Jet Set material is highly isotropic, as all of the three tests result in similar curves. Meanwhile, the friction between sponge and the Jet Set material is more anisotropic, as Figure 9d shows. To understand the nonlinearity in friction, we adjust the weight load and record the average friction force over time. The result in Figure 9e shows that the friction between sheepskin and the Rib Knit material is more nonlinear, while the friction between plastic foam and the Polyester material is more linear, largely due to its smoothness.

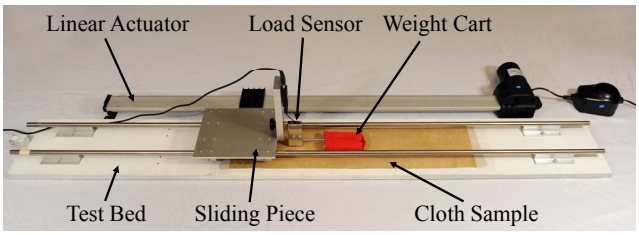

Figure 7: *The friction measurement device.*

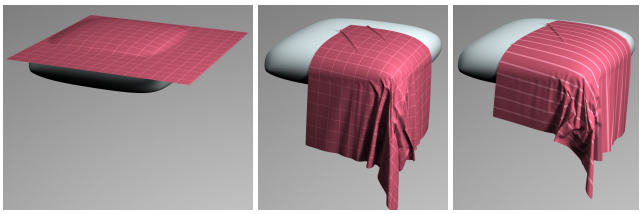

(a) Initial configuration (b) A Polyester sheet (c) A Jet Set sheet

Figure 8: *Friction effects. A Polyester sheet and a Jet Set sheet exhibit different friction effects, when they both fall onto the same sponge cushion as shown in (a). The Polyester sheet slides equally fast in the warp and weft directions as (b) shows, due to isotropic friction. Meanwhile, the Jet Set sheet slides more toward to the right side as (c) shows, because of anisotropic friction.*

Our existing dataset includes the ten cloth materials in the cloth elasticity database developed by Wang and collaborators [2011] and five deformable body materials: sponge, cotton, plastic foam, raw sheepskin, and waxed sheepskin. For each pair of materials, we first test the friction forces in 0°, 45°, and 90° directions under the same load. If they appear to be similar, we simply assume that their friction is isotropic. A large number of tests are needed when the friction force is both anisotropic and nonlinear. Fortunately, such cases do not happen often, as our experiment shows.

5.2 Friction Model

Many existing physically based simulators use Coulomb's law to model the dynamic friction force between two objects: $\mathbf{f}^{\mathrm{f}} = -\mu|\mathbf{f}^{\mathrm{n}}|\mathbf{v}^{\mathrm{t}}/|\mathbf{v}^{\mathrm{t}}|$, in which μ is a constant friction coefficient, $\mathbf{v}_{\mathrm{t}}$ is the tangent velocity, and $\mathbf{f}^{\mathrm{n}}$ is the pressure force between the two objects in the normal direction. In our system, $\mathbf{f}^{\mathrm{n}}$ is obtained from the collision impulse calculated in Subsection 4.2. Since Coulomb's law is only an approximation while real-world friction is more complex, we propose a new friction model based on the frictional data captured in Subsection 5.1.

We first consider the nonlinearity. Assuming that the friction between two objects behaves isotropically, we can use the load-force curve to obtain the frictional force immediately:

$$\mathbf{f}^{\mathrm{f}} = -f(|\mathbf{f}^{\mathrm{n}}|)\frac{\mathbf{v}^{\mathrm{t}}}{|\mathbf{v}^{\mathrm{t}}|}, \tag{1}$$

in which $f(\cdot)$ is the load-force function as in Figure 9e. The situation gets complex when the friction is anisotropic, since we need to consider different load-force relationships in different directions. Here we make a few assumptions to simplify our model. Firstly, we assume that the friction is symmetric. In other words, when an object slides in one direction, the magnitude of the received force should be the same as the force magnitude when the object slides in the opposite direction. Secondly, we assume that the friction force

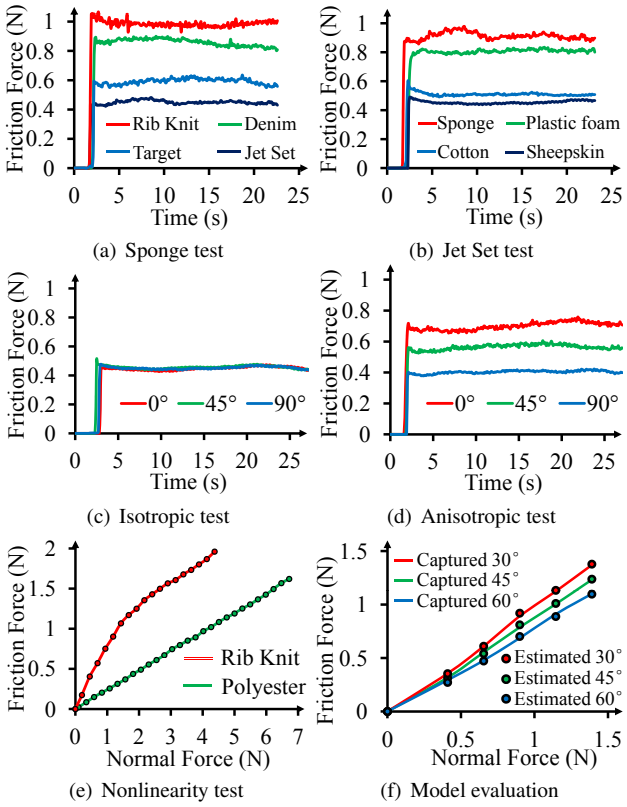

(a) Sponge test (b) Jet Set test

(c) Isotropic test (d) Anisotropic test

(e) Nonlinearity test (f) Model evaluation

Figure 9: *Friction test results. Our experiment shows that the friction force is affected by the combination of different cloth materials in (a) and deformable body materials in (b). Even when testing the same materials, the friction behavior can vary in different sliding directions as (d) shows, and the relationship between the pressure force and the friction force can be nonlinear as (e) shows. Our friction model approximates these behaviors as shown in (f).*

is always in the opposite direction of the tangent velocity. Last but not least, we assume that the friction is orthotropic, so the friction force is symmetric to two orthogonal axes. This is a reasonable assumption, since most deformable body materials that we tested are isotropic and most cloth materials are orthotropic. Under these assumptions, we propose an anisotropic nonlinear friction model as:

$$\mathbf{f}^{\mathrm{f}} = -\mathbf{u}^{\mathsf{T}}\begin{pmatrix} f_{00}(|\mathbf{f}^{\mathrm{n}}|) & f_{01}(|\mathbf{f}^{\mathrm{n}}|) \\ f_{01}(|\mathbf{f}^{\mathrm{n}}|) & f_{11}(|\mathbf{f}^{\mathrm{n}}|) \end{pmatrix}\mathbf{u}\frac{\mathbf{v}^{\mathrm{t}}}{|\mathbf{v}^{\mathrm{t}}|}, \tag{2}$$

in which $\mathbf{u}$ is the normalized 2D velocity direction in the material space, and $f_{00}(\cdot)$, $f_{01}(\cdot)$, and $f_{11}(\cdot)$ are three nonlinear functions describing the friction anisotropy. We obtain these three functions by solving a linear equation, using the load-force curves in different orientations. When the deformable body is isotropic and the cloth is orthotropic, we assume that the maximum and minimum friction forces are in the warp and weft directions. So $f_{01}(\cdot)$ is zero, and $f_{00}(\cdot)$ and $f_{11}(\cdot)$ correspond to the 0° and 90° load-force curves immediately. Figure 9f compares the captured load-force curves with the estimated curves in 30°, 45° and 60°, using such a model. Figure 8 demonstrates the effects of our friction model in animation.

The nonlinearity in friction behaviors is often due to slight compressibility of the material surface. We find it to be important, but it was not considered in the previous model by Pabst and collaborators [2009]. We also note that friction behaviors cannot be easily determined by the two material properties. For example, the Jet-

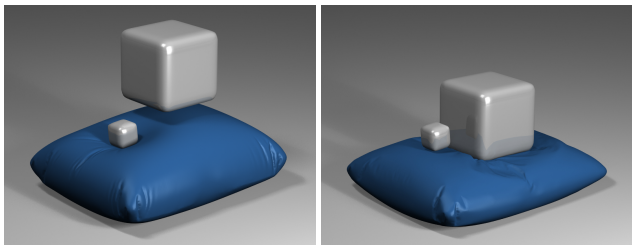

(a) Before contact (b) After contact

Figure 10: *The air pressure effect. Before the large cube hits the pillow, the pillow is filled with air as (a) shows. After the contact, the propagated air pressure causes the small cube to jump and air to penetrate through the pillow cover as shown in (b).*

Set/sponge friction is anisotropic, while the Jet-Set/sheepskin friction and the Rib-Knit/sponge friction are both isotropic. It would be difficult to identify this anisotropy, without doing actual friction tests. Finally, our model in Equation 2 cannot handle self frictions of highly anisotropic materials. To solve this problem, at least two tensors will be needed as Pabst and collaborators [2009] did.

6 Air Effects

The air layer functions as a buffer between the cloth layer and the deformable body layer. Its effect is often visible on the cloth cover, due to its air pressure forces. Since the air layer is computationally expensive to animate by fluid simulation, we develop a simple technique to generate its effects using an air mass field as shown in Figure 10 and 11. While this technique assumes that the deformable body is airproof, it provides a good approximation to porous deformable material cases as well, such as cotton and sponge.

According to the ideal gas law, $PV = nRT$, in which P is the pressure, V is the volume, n is the amount of air, R is a constant, and T is the temperature. When the temperature is constant, we simply treat nRT as an air mass constant and we define the air mass between a cloth vertex i and the deformable body as Q_i. The pressure at vertex i can then be calculated as $P_i = Q_i/(A_i d_i)$, in which A_i is the vertex area, d_i is the distance from i to the body, and $A_i d_i$ is an approximation to the air volume between i and the body. Here we assume cloth does not form large folds on itself, which is a reasonable assumption since air effects can flatten the cloth cover. Although the air volume can be better approximated as $A_i d_i \cos\theta_i$, in which θ_i is the angle between the cloth normal at i and the body surface normal, instability issues may occur when θ_i gets close to $\pi/2$ and P_i becomes arbitrarily large. So we do not use this formula in practice.

Let $P_{\text{atm}} = 1.01\text{kPa}$ be the atmospheric pressure, we compute the air pressure force at i as:

$$\mathbf{f}_i^{\text{air}} = (P_i - P_{\text{atm}}) A_i \mathbf{N}_i, \tag{3}$$

where $\mathbf{N}_i$ is vertex i's outward normal. The deformable body receives air pressure forces in the same way, except that a force may not be defined at a body vertex. In that case, we use the barycentric weights to distribute it to triangle vertices. The key component in this method is the air mass update step, and we propose to handle it using two models.

Air Transfer. Researchers in textile engineering have studied air permeability of different fabrics for decades, and they developed the Shirley air permeability test, by measuring the amount of air traveling through cloth under a given pressure difference. A dataset of such measured data can be found in [Cay et al. 2007]. Since the rate of a fluid traveling through a porous medium is proportional to the pressure difference as Darcy's law shows, we can formulate the pressure change caused by air transfer as:

$$\frac{\partial Q_i}{\partial t} = \sigma \frac{P_{\text{atm}} - Q_i/(A_i d_i)}{\Delta P} A_i P_{\text{atm}}, \tag{4}$$

in which the air permeability coefficient σ is the amount of air volume (under the atmospheric pressure) moving through cloth per unit area per second, and $\Delta P = 0.2\text{kPa}$ is the pressure difference according to the BSI standard.

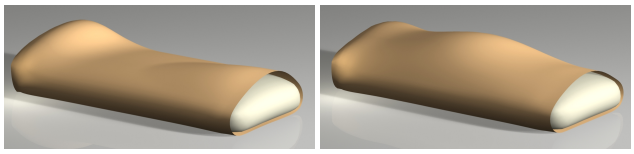

Figure 11: *Waves caused by air propagation. Wind enters a pillow on the left side and leaves the pillow on the right side, forming wavy effects on the pillow cover.*

Air Propagation. Air can also travel within the air layer, when the pressure is not uniform. Let i and j be two neighboring cloth vertices and if $P_i \neq P_j$, then:

$$\frac{\partial^2 Q_i}{\partial t^2} = k\left(\frac{Q_j}{A_j d_j} - \frac{Q_i}{A_i d_i}\right) s_{ij} = -\frac{\partial^2 Q_j}{\partial t^2}, \tag{5}$$

in which k is a propagation speed coefficient and s_{ij} is the contacting area. We calculate s_{ij} as $c_{ij}(d_i + d_j)/2$, in which c_{ij} is the mass-center distance of the two triangles adjacent to edge ij.

System. We use an implicit solver to update the air mass field caused by the two steps. This gives a matrix system $\mathbf{M}\mathbf{Q}^{t+1} = \mathbf{b}$, in which $m_{ii} = 1 + \frac{\sigma P_{\text{atm}} \Delta t}{\Delta P d_i^{t+1}} + \frac{k\Delta t^2}{A_i d_i^{t+1}} \sum_j s_{ij}^{t+1}$, $m_{ij} = -\frac{k s_{ij}^{t+1} \Delta t^2}{A_j d_j^{t+1}}$, and $b_i = Q_i^t \left(2 + \frac{\sigma P_{\text{atm}} \Delta t}{\Delta P d_i^{t+1}}\right) - Q_i^{t-1}$. Since $\mathbf{M}$ is asymmetric but diagonally dominant, we solve this system using the bi-conjugate gradient stabilized method. The result $\mathbf{Q}^{t+1} = \{Q_0^{t+1}, Q_1^{t+1}, ..., Q_n^{t+1}\}$ is the updated air mass field at time $t + 1$. To handle open cloth meshes, We simply enforce the air mass at boundary vertex i as: $Q_i^{t+1} = P_{\text{atm}} A_i d_i^{t+1}$, so its pressure stays at P_{atm}.

7 Results

(Please refer to the supplemental video for animation results.) Our experiments are tested on a PC with an Intel Core i7-2600 3.4GHz 4-core CPU. The cloth material properties are chosen from the cloth elasticity database given by Wang and collaborators [2011]. For self collisions, we used the continuous collision detection technique developed by Bridson and collaborators [2002]. We used two external forces in our examples: the gravity force, which is applied on both cloth and deformable bodies; and a linear air drag force, which is applied on cloth only. The time step varies from 0.2ms to 1ms, and the animations are rendered at 30FPS.

Rotating sphere. This example (in Figure 1) reveals the difference among cloth, a deformable body, and a three-layer object in their animation behaviors. The three objects drop onto a sphere and then the sphere gradually rotates, causing intensive collisions. Our system robustly detects collisions between cloth and the inner body as Figure 1c shows. Here the cloth layer contains 21K vertices and the inner body contains 11K tetrahedra. The total computational cost spent in every time step is 0.25s, including both dynamic solver costs and collision costs.

(a) Cloth cover (b) Bedding set (c) Down vest

Figure 12: *Animation examples that demonstrate the robustness and efficiency of our system.* *(The car model ©Alexander Lashko)*

Cloth cover. To test the performance of our collision handling algorithm in open cloth cases, we simulate the cloth cover example in Figure 12a. This example shows that our algorithm is robust and efficient, even when the cloth cover slides a long distance over a bumpy car surface. The car surface contains 18K vertices and the cloth contains 80K vertices. The average computational cost per time step is 0.05s.

Bedding set. Our system can also animate complex scenes, such as a whole bedding set. This scene contains a cloth sheet, a comforter, and a pillow, as Figure 12b shows. For simplicity, we use our collision algorithm to handle collisions among these objects as well. There are totally 81K vertices used in this example and each time step takes 0.07s to simulate.

Down vest. In this example (in Figure 12c), we demonstrate the ability of our techniques to simulate winter clothes, such as this down vest dressed on a virtual character. This down vest model is made of an inner body with 5K vertices and a cloth cover with 117K vertices. To save the computational cost, we adaptively sample the cloth cover so that fewer vertices are used on the inner side. We do not handle the interactions between the inner cloth vertices and the inner body. The inner cloth vertices are simply glued onto the inner body by constraints. Since we do not have real-world deformable body material properties for this example, the inner body looks slightly stiffer than it should be. We plan to improve this in the future. It takes 0.37s to simulate each time step in this example.

8 Limitations

Our collision detection algorithm cannot handle self collisions. As a discrete algorithm, it suffers from tunneling artifacts when vertices are moving too fast or when deformable bodies are too thin. Its efficiency relies on the smoothness and the resolution of inner body surfaces. In the worst case, its computational cost will be the same as an algorithm that calculates the vertex-body distance using all deformable body triangles. Our current friction experiment cannot capture static frictions well. The proposed dynamic friction model assumes that the friction behavior is symmetric and orthotropic, therefore, it cannot handle self frictions of highly anisotropic materials or materials with oriented fibers, such as fur. Our air layer model assumes that cloth does not fold on itself and deformable bodies are airproof. It does not consider pressure variations in the normal direction, nor air flows blocked by external objects.

9 Conclusions and Future Work

In this paper, we developed efficient and accurate algorithms to handle friction and air effects between cloth and deformable bodies. Our collision handling algorithm demonstrated the effectiveness of using the surface traversal technique in collision detection. The proposed algorithm is useful not only in our system, but also in similar multi-layer cases. For example, it can efficiently handle collisions among multiple winter clothing pieces. Our friction measurement experiment allows us to model both cloth-body frictions and self frictions of cloth, the latter of which are more complex in the real world. Last but not least, we showed that the air effect can be simulated without solving fluid dynamics and the use of real-world data can help improve the realism of cloth simulation.

Looking into the future, our immediate plan is to use GPU acceleration in our implementation. To verify the accuracy of our air layer model, we plan to compare it with fluid simulation results. We are interested in improving our measurement device, so that it can capture static frictions better. We will investigate more into the friction model and its relationship with material properties, such as wetness and roughness. By testing more cloth and deformable body materials, we hope that we can build a comprehensive friction database for future graphics research in cloth simulation.

Acknowledgments

We thank James F. O'Brien and Ravi Ramamoothi for inspiring suggestions on this work. We also thank NVIDIA for supporting our work through equipment and funding.

References

Ainsley, S., Vouga, E., Grinspun, E., and Tamstorf, R. 2012. Speculative parallel asynchronous contact mechanics. *ACM Trans. Graph. (SIGGRAPH Asia) 31*, 6 (Nov.), 151:1–151:8.

Baraff, D., Witkin, A., and Kass, M. 2003. Untangling cloth. *ACM Trans. Graph. (SIGGRAPH) 22* (July), 862–870.

Bhat, K. S., Twigg, C. D., Hodgins, J. K., Khosla, P. K., Popović, Z., and Seitz, S. M. 2003. Estimating cloth simulation parameters from video. In *Proc. of SCA*, 37–51.

Bickel, B., Bächer, M., Otaduy, M. A., Matusik, W., Pfister, H., and Gross, M. 2009. Capture and modeling of non-linear heterogeneous soft tissue. *ACM Trans. Graph. (SIGGRAPH) 28*, 3 (July), 89:1–89:9.

Bridson, R., Fedkiw, R., and Anderson, J. 2002. Robust treatment of collisions, contact and friction for cloth animation. *ACM Trans. Graph. (SIGGRAPH) 21*, 3 (July), 594–603.

Brochu, T., Edwards, E., and Bridson, R. 2012. Efficient geometrically exact continuous collision detection. *ACM Trans. Graph. (SIGGRAPH) 31*, 4 (July), 96:1–96:7.

Cay, A., Vassiliadis, S., Rangoussi, M., and Tarakcioglu, I. 2007. Prediction of the air permeability of woven fabrics using neural networks. *International Journal of Clothing Science and Technology 19*, 18–35.

Coros, S., Martin, S., Thomaszewski, B., Schumacher, C., Sumner, R., and Gross, M. 2012. Deformable objects alive! *ACM Trans. Graph. (SIGGRAPH) 31*, 4 (July), 69:1–69:9.

Deben, 2013. Biaxial tensile stage for textiles and polymers, January. http://www.deben.co.uk/details.php?id=11.

Faure, F., Gilles, B., Bousquet, G., and Pai, D. K. 2011. Sparse meshless models of complex deformable solids. *ACM Trans. Graph. (SIGGRAPH) 30*, 4 (July), 73:1–73:10.

Frazier, 2013. Differential pressure air permeability tester, January. http://www.frazierinstrument.com/products/fap/fap.html.

Gascón, J., Zurdo, J. S., and Otaduy, M. A. 2010. Constraint-based simulation of adhesive contact. In *Proc. of SCA*, 39–44.

Guendelman, E., Selle, A., Losasso, F., and Fedkiw, R. 2005. Coupling water and smoke to thin deformable and rigid shells. *ACM Trans. Graph. (SIGGRAPH) 24*, 3 (July), 973–981.

Harmon, D., Vouga, E., Smith, B., Tamstorf, R., and Grinspun, E. 2009. Asynchronous contact mechanics. *ACM Trans. Graph. (SIGGRAPH) 28*, 3 (July), 87:1–87:12.

Huber, M., Pabst, S., and Straßer, W. 2011. Wet cloth simulation. In *ACM SIGGRAPH 2011 Posters*, 10:1–10:1.

Jimenez, S., and Luciani, A. 1993. Animation of interacting objects with collisions and prolonged contacts. In *Proc. of the IFIP Working Group 5.10*, 129–141.

KATO Tech, 2013. KES-FB2-AUTO-A bending tester, January. http://english.keskato.co.jp/products/kes_fb2.html.

KATO Tech, 2013. KES-G2 strip biaxial tensile tester, January. http://english.keskato.co.jp/products/kes_g2.html.

KATO Tech, 2013. KES-SE friction tester, January. http://english.keskato.co.jp/products/kes_se.html.

Kauer, M., Vuskovic, V., Dual, J., Szekely, G., and Bajka, M. 2002. Inverse finite element characterization of soft tissues. *Medical Image Analysis 6*, 3, 257–287.

Kunitomo, S., Nakamura, S., and Morishima, S. 2010. Optimization of cloth simulation parameters by considering static and dynamic features. In *ACM SIGGRAPH 2010 Posters*, 15:1–15:1.

Lang, J., Pai, D., and Woodham, R. J. 2002. Acquisition of elastic models for interactive simulation. *International Journal of Robotics Research 21*, 8, 713–733.

Lauterbach, C., Mo, Q., and Manocha, D. 2010. gProximity: Hierarchical GPU-based operations for collision and distance queries. In *Proc. of Eurographics*, vol. 29, 419–428.

Lenaerts, T., Adams, B., and Dutré, P. 2008. Porous flow in particle-based fluid simulations. *ACM Trans. Graph. (SIGGRAPH) 27*, 3 (Aug.), 49:1–49:8.

Miguel, E., Bradley, D., Thomaszewski, B., Bickel, B., Matusik, W., Otaduy, M. A., and Marschner, S. 2012. Data-driven estimation of cloth simulation models. In *Proc. of Eurographics*, vol. 31.

Müller, M., Dorsey, J., McMillan, L., Jagnow, R., and Cutler, B. 2002. Stable real-time deformations. In *Proc. of SCA*, 49–54.

Pabst, S., Thomaszewski, B., and Strasser, W. 2009. Anisotropic friction for deformable surfaces and solids. In *Proc. of SCA*, 149–154.

Pai, D. K., Doel, K. v. d., James, D. L., Lang, J., Lloyd, J. E., Richmond, J. L., and Yau, S. H. 2001. Scanning physical interaction behavior of 3D objects. In *Proc. of SIGGRAPH 98*, Annual Conference Series, 87–96.

Provot, X. 1997. Collision and self-collision handling in cloth model dedicated to design garments. In *Computer Animation and Simulation*, 177–189.

Qualitest, 2013. Coefficient of friction (COF) tester, January. http://www.worldoftest.com/cof.htm.

Schoner, J. L., Lang, J., and Seidel, H.-P. 2004. Measurement-based interactive simulation of viscoelastic solids. In *Proc. of Eurographics*, vol. 23, 547C–556.

Schvartzman, S. C., Pérez, A. G., and Otaduy, M. A. 2010. Star-contours for efficient hierarchical self-collision detection. *ACM Trans. Graph. (SIGGRAPH) 29* (July), 80:1–80:8.

SDL Atlas, 2013. Air permeability tester, January. http://www.sdlatlas.com/consumable/58/.

Shinar, T., Schroeder, C., and Fedkiw, R. 2008. Two-way coupling of rigid and deformable bodies. In *Proc. of SCA*, 95–103.

Sifakis, E., Marino, S., and Teran, J. 2008. Globally coupled collision handling using volume preserving impulses. In *Proc. of SCA*, 147–153.

Stam, J. 2009. Nucleus: Towards a unified dynamics solver for computer graphics. In *11th IEEE International Conference on Computer-Aided Design and Computer Graphics*.

Taber Industries, 2013. Fabric stiffness tester, January. http://www.taberindustries.com/fabric-stiffness.

Tang, M., Manocha, D., Yoon, S.-E., Du, P., Heo, J.-P., and Tong, R.-F. 2011. VolCCD: Fast continuous collision culling between deforming volume meshes. *ACM Trans. Graph. 30*, 5 (Oct.), 111:1–111:15.

Textest, 2013. Air Permeability Tester FX 3300 LabAir IV, January. http://www.textest.ch/pages_en/3300-IV_en.htm.

Thomaszewski, B., Pabst, S., and Straßer, W. 2008. Asynchronous cloth simulation. In *Proc. of Computer Graphics International*.

Volino, P., Magnenat-Thalmann, N., and Faure, F. 2009. A simple approach to nonlinear tensile stiffness for accurate cloth simulation. *ACM Trans. Graph. 28*, 4 (September), 105:1–105:16.

Wang, H., O'Brien, J. F., and Ramamoorthi, R. 2011. Data-driven elastic models for cloth: Modeling and measurement. *ACM Trans. Graph. (SIGGRAPH) 30*, 4 (July), 71:1–71:12.

Wicke, M., Lanker, H., and Gross, M. 2006. Untangling cloth with boundaries. In *Proc. of Vision, Modeling, and Visualization*, 349–356.

Zheng, C., and James, D. L. 2012. Energy-based self-collision culling for arbitrary mesh deformations. *ACM Trans. Graph. (SIGGRAPH) 31*, 4 (July), 98:1–98:12.